Journal Name

ARTICLE TYPE

Cite this: DOI: 00.0000/xxxxxxxxxx

Supplemental Material for "Origin of ferromagnetism and the effect of dopings in Fe_3GeTe_2"

Seung Woo Jang,[a] Hongkee Yoon,[a] Min Yong Jeong,[a] Siheon Ryee,[a] Heung-Sik Kim,[b] and Myung Joon Han*[a]

Received Date
Accepted Date

DOI: 00.0000/xxxxxxxxxx

[a]*Department of Physics, Korea Advanced Institute of Science and Technology (KAIST), Daejeon 34141, Republic of Korea; E-mail: mj.han@kaist.ac.kr*
[b]*Department of Physics, Kangwon National University, Chuncheon-Si, Gangwon-Do, 24341 Republic of Korea.*

† Electronic Supplementary Information (ESI) available: [details of any supplementary information available should be included here]. See DOI: 00.0000/00000000.

1 The lattice parameters and rPW86' functional

Table 1 shows the optimized lattice parameters for the undoped bulk FGT obtained by various XC functionals. The experimental data is the value influenced by Fe defects [1,2]. We note that 'rPW86' functional significantly overestimates both a and c.

2 Supplementary plot for the magnetic couplings

Here we replot the magnetic coupling constants J as a function of inter-atomic distance without taking the coordination number into account, serving as a supplementary plot for Fig. 1 and 2 in the main manuscript. Figure 1(a) and (b) presents the intra- and inter-layer interaction, respectively, for $Fe_{3.0}GeTe_2$ (no defect). Figure 1(c) and (d) are for $Fe_{2.75}GeTe_2$ (Fe defect).

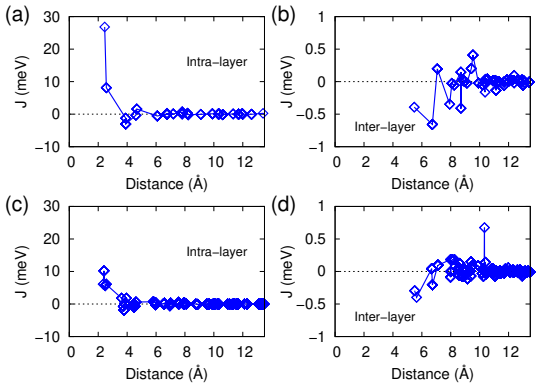

Fig. 1 The calculated magnetic interactions for (a, b) $Fe_{3.0}GeTe_2$ and (c, d) $Fe_{2.75}GeTe_2$. (a, c) and (b, d) shows the intra- and the inter-layer couplings, respectively.

3 Further analysis on the magnetic interactions

To understand the origin of inter-layer AFM coupling, it is insightful to investigate the magnetic interactions in between the two inequivalent Fe sites, namely, Fe_I and Fe_{II}. Figure 2 shows the calculated magnetic coupling in between Fe_{II} and Fe_{II} (green), Fe_I and Fe_{II} (blue), and Fe_I and Fe_I (red) within the layer (a) and across the layer (b). Note that the Fe_I-Fe_I coupling is the dominant inter-layer AFM interaction that makes this material AFM; see Fig. S2(b). By introducing Fe defect or doping, this AFM interaction is markedly suppressed, thereby stabilizing the inter-layer FM order. In $Fe_{2.75}GeTe_2$, the moment size of Fe_I decreases by doping from 1.85 μ_B to 0.69 μ_B and 1.63 μ_B for Fe_I site near and far from the defect site, respectively. On the other hand, the Fe_{II} moment increases from 1.03 μ_B to 1.30 μ_B. Since the interlayer Fe_I-Fe_I coupling is the main AFM channel while the Fe_{II}-Fe_I and Fe_{II}-Fe_{II} coupling is FM, this trend of moment size change drives the interlayer magnetic interaction from AFM (at zero doping) to FM (at finite doping). See the next page Figure 3(b) in Sec. 4.

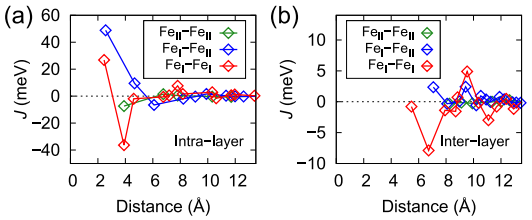

Fig. 2 The calculated intra-layer (a) and inter-layer (b) magnetic couplings J for stoichiometric FGT (with no defect, no doping). The interactions between two different Fe sites are analyzed and compared; the green, blue, and red color refers to the interaction of J(Fe_{II}-Fe_{II}), J(Fe_I-Fe_{II}), and J(Fe_I-Fe_I), respectively.

	Optimized in FM									
	LDA	PBEsol	D2	D3(Grimme)	D3(BJ)	TS	dDsC	optB86b	rPW86	Exp. [1]
a (Å)	3.90	3.98	4.00	4.02	4.01	4.01	4.02	4.02	4.17	3.99
c (Å)	15.87	16.25	16.48	16.18	15.98	15.75	16.28	16.38	17.46	16.33

Table 1 The structural parameters of FGT optimized by 9 different XC functionals.

4 Analysis of the orbital-decomposed inter-layer couplings and the electronic structures

In order to have further insight on the origin of AFM-to-FM transition induced by Fe defect, we perform the electronic structure analysis. Since the major inter-layer AFM interaction in stoichiometric FGT (undoped; no defect) is in between two Fe_I sites (see Sec. 3 of Supplemental Material), we focus on Fe_I. Fig. 3(a) shows that the major orbital path for AFM inter-layer coupling is the interaction in between two $d_{yz,zx}$ orbitals. The corresponding projected density of states (PDOS) are presented in Fig. 3(c) where the red colored line represents the $d_{yz,zx}$ states. Due to the crystal symmetry of this material, d_{xy} and d_{yz} states are identical with $d_{x^2-y^2}$ and d_{zx}, respectively. We also found that the other inter-orbital couplings (*e.g.*, $J_{d_{xy}\text{-}d_{yz,zx}}$, $J_{d_{xy}\text{-}d_{z^2}}$,... etc) are negligible and therefore not presented.

Importantly, by introducing Fe defect, this AFM interaction is largely suppressed as shown in Fig. 3(b), and the inter-layer coupling becomes FM as shown in the main manuscript. In PDOS, most noticeable is the $d_{yz,zx}$ states whose down-spin components are peaked across the Fermi level for the case of $Fe_{3.0}GeTe_2$ (see Fig. 3(c); indicated by the red arrow). In $Fe_{2.75}GeTe_2$, this state is largely pushed down below the Fermi level (see Fig. 3(d); indicated by the red arrow). This analysis implies that this electronic structure change of $d_{yz,zx}$ is responsible for the suppressed AFM coupling in the presence of defect or doping. The same behavior is also found in the calculation with varying system charge.

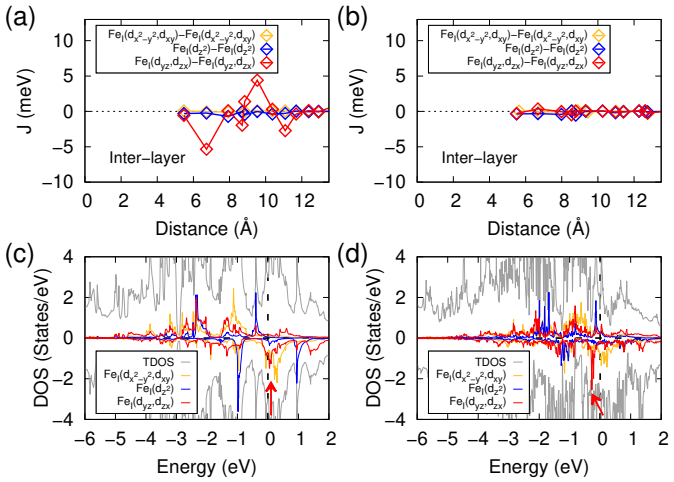

Fig. 3 (a, b) The orbital-decomposed inter-layer magnetic couplings in between two Fe_I sites without (a) and with (b) Fe defects. Due to the crystal symmetry, d_{xy} and d_{yz} states are identical with $d_{x^2-y^2}$ and d_{zx}, respectively. Three different colors refer to the three different types of orbital-decomposed interactions. Other inter-orbital interactions (which are not shown here) are found to be negligible. (c, d) The calculated PDOS of Fe_I without (a) and with (b) Fe defect. The same color codes are used for three distinctive orbital states. The gray lines represent the total DOS. Note that Fe sites in this system is in the environment far from the ideal octahedral crystal field. Thus the x, y, z coordinate is defined to be arbitrary global axes.

5 FM stabilization energy and T_c trend

Figure 4 shows another meaningful indication that Fe defect and hole doping are of key importance to understand the ferromagnetism in FGT. The calculated total energy difference between FM and non-magnetic (NM) phase is presented as a function of hole doping. Note that this energy difference can be a measure of FM T_c. It monotonically decreases as the hole doping increases, which is in good agreement with the T_c trend observed in experiment[2]. Therefore, this result provides a further evidence that the ferromagnetism of FGT is governed by Fe defect and hole doping.

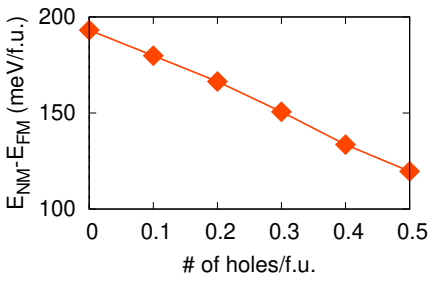

Fig. 4 The calculated total energy difference between FM and NM solutions as a function of hole doping.

6 The calculated magnetic moment for doped FGT

The calculated magnetic moment is another important indication of that the residing holes or Fe defects affect the magnetic property of FGT. Figure 5 presents the calculated Fe moment (the averaged value of Fe_I and Fe_{II}) by several different GGA-based XC functionals. It has been reported that the use of GGA functional significantly overestimates the magnetic moment[3,4]. It leads researchers to adopt LDA (plus vdW correction) which gives the better agreement with experiments. Figure 5 clearly shows that, by taking into account of hole dopings, the moment is noticeably reduced, and importantly, the results of all XC functionals fall into the range of experiment[1–3,5]. For the case of electron-doped FGT, there is no experimental value reported. The calculated magnetic moment is ∼1.4–1.6 μ_B.

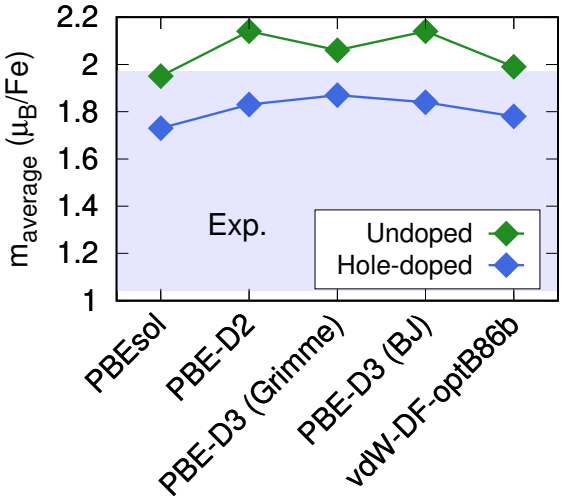

Fig. 5 The calculated magnetic moment of bulk FGT by GGA-based XC functionals. The green and blue symbols represent the results of undoped and hole-doped FGT, respectively. We considered 0.5 holes per f.u., which corresponds to the FM region of phase diagram. The blue-shaded area shows the region of experimental values.[1–3,5].

7 z_{Li} and the electron doping

In the main manuscript, we present the effect of electron doping in terms of Li height, $1/z_{Li}$. Of course, it can also be presented as a function of Mulliken charge. Figure 6 shows the amount of doped or transferred electrons from Li to the bi-layer FGT. It is proportional to the inverse height of Li atom.

We also tried to simulate the electron doping situation in different ways by, for example, using both system charge and Li insertion. It is found that the structure becomes unstable; e.g., the interlayer distance becomes unphysically large, and microscopically, the main difference is that the electrons are distributed widely over the layers. It is likely related to the fact that this material gets easily hole-doped (i.e., Fe-defected) but no report on the electron doping. The recent gating experiment is the only exception.

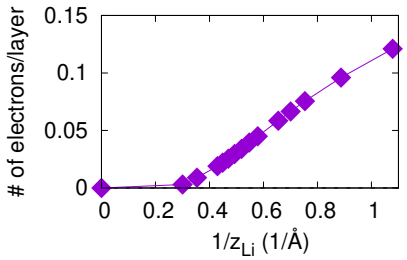

Fig. 6 The number of doped electrons (Mulliken charge) as a function of the inverse distance between surface Te and Li atom.

8 The k-mesh dependence of total energy

It is important to adopt a large enough number of **k** points. As Figure 7 shows, 9×9×4 mesh is not enough which incorrectly gives the FM solution as the ground state. Using the denser **k** meshes gives rise to the AFM ground state.

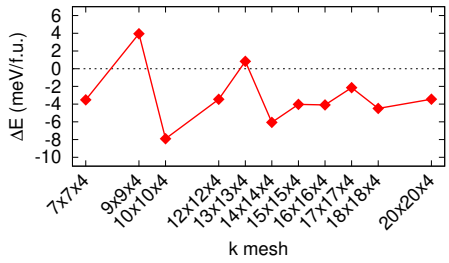

Fig. 7 The calculated total energy difference ($\Delta E = E_{\mathrm{AFM}} - E_{\mathrm{FM}}$) for the undoped FGT with different **k** meshes.

9 Defect formation energy

It is known from experiments that stoichiometric $Fe_{3.0}GeTe_2$ can hardly be synthesized, and some amount of Fe defects does exist [1,2,2,3,6–8]. It would be instructive to calculate the defect formation energy (E_f) for $Fe_{3-x}GeTe_2$. Considering that the system is metallic, we adopted the following equation [9];

$$E_f = E^{\mathrm{FGT}}_{\mathrm{x=0.125}} + E^{\mathrm{bcc\text{-}Fe}} - E^{\mathrm{FGT}}_{\mathrm{x=0.0}} \quad (1)$$

where $E^{\mathrm{FGT}}_{\mathrm{x=0.125}}$, $E^{\mathrm{bcc\text{-}Fe}}$, and $E^{\mathrm{FGT}}_{\mathrm{x=0.0}}$ is the calculated total energy of $Fe_{2.875}GeTe_2$, bcc Fe, and $Fe_{3.0}GeTe_2$, respectively. In our supercell, the removal of one Fe atom corresponds to $x = 0.125$ which is in the range of experimental values. Experimentally, it is known that $0.11 < x < 0.36$ for single crystal or powder, and $0.03 < x < 0.31$ for polycrystalline sample [2]. Fe_{II} is considered as the defect site following the previous experimental report [1].

The calculated formation energy $E_f = -0.267$ eV. The negative formation energy implies that the Fe deficiency is likely present in any sample, which is consistent with experimental reports [1–3,6–8]. The negative value is remedied by adopting GGA ($E_f = +0.241$ eV) which indicates the LDA limitation.

10 Dynamic stability of $Fe_{2.75}GeTe_2$

To examine the dynamic stability of Fe-deficient FGT, we examined the phonon dispersion. Fig. 8 clearly shows that $Fe_{2.75}GeTe_2$ is dynamically stable just as for the case of stoichiometric Fe_3GeTe_2 [4].

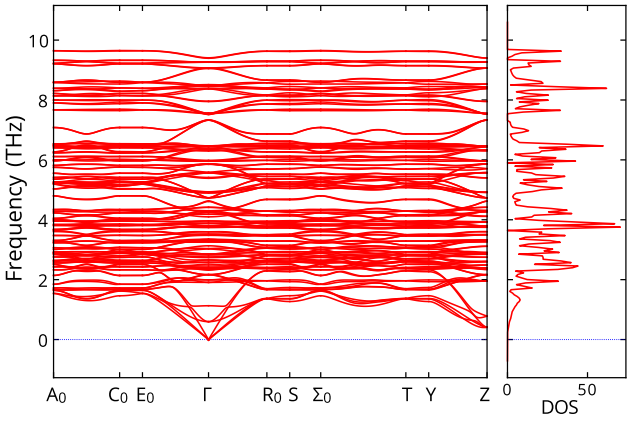

Fig. 8 The calculated phonon dispersion of $Fe_{2.75}GeTe_2$ along high symmetry lines and the phonon density of states. We used the $2 \times 2 \times 1$ times larger supercell which contains the 22 Fe atoms (two Fe_{II} defects).

Notes and references

1 H.-J. Deiseroth, K. Aleksandrov, C. Reiner, L. Kienle and R. K. Kremer, *Eur. J. Inorg. Chem.*, 2006, **2006**, 1561–1567.

2 A. F. May, S. Calder, C. Cantoni, H. Cao and M. A. McGuire, *Phys Rev B*, 2016, **93**, 014411.

3 J.-X. Zhu, M. Janoschek, D. S. Chaves, J. C. Cezar, T. Durakiewicz, F. Ronning, Y. Sassa, M. Mansson, B. L. Scott, N. Wakeham, E. D. Bauer and J. D. Thompson, *Phys. Rev. B*, 2016, **93**, 144404.

4 H. L. Zhuang, P. R. C. Kent and R. G. Hennig, *Phys Rev B*, 2016, **93**, 134407.

5 B. Chen, J. Yang, H. Wang, M. Imai, H. Ohta, C. Michioka, K. Yoshimura and M. Fang, *J Phys Soc Jpn*, 2013, **82**, 124711.

6 V. Y. Verchenko, A. A. Tsirlin, A. V. Sobolev, I. A. Presniakov and A. V. Shevelkov, *Inorg Chem*, 2015, **54**, 8598–8607.

7 Y. Liu, V. N. Ivanovski and C. Petrovic, *Phys Rev B*, 2017, **96**, 144429.

8 Y. Liu, E. Stavitski, K. Attenkofer and C. Petrovic, *Phys Rev B*, 2018, **97**, 165415.

9 C. Freysoldt, B. Grabowski, T. Hickel, J. Neugebauer, G. Kresse, A. Janotti and C. G. Van de Walle, *Rev. Mod. Phys.*, 2014, **86**, 253–305.